Development 128, 5017-5029 (2001)
Printed in Great Britain © The Company of Biologists Limited 2001
DEV4560

Hmx2 homeobox gene control of murine vestibular morphogenesis

Weidong Wang[1], Edwin K. Chan[2], Shira Baron[2], Thomas Van De Water[2] and Thomas Lufkin[1,*]

[1]Brookdale Center for Developmental and Molecular Biology, Mount Sinai School of Medicine, One Gustave L. Levy Place, New York, NY 10029-6574, USA
[2]Departments of Otolaryngology and Neuroscience, Albert Einstein College of Medicine, 1410 Morris Park Avenue, Bronx, NY 10461, USA
*Author for correspondence (e-mail: thomas.lufkin@mssm.edu)

Accepted 18 September 2001

SUMMARY

Development of the vertebrate inner ear is characterized by a series of genetically programmed events involving induction of surface ectoderm, preliminary morphogenesis, specification and commitment of sensory, nonsensory and neuronal cells, as well as outgrowth and restructuring of the otocyst to form a complex labyrinth. *Hmx2*, a member of the *Hmx* homeobox gene family, is coexpressed with *Hmx3* in the dorsolateral otic epithelium. Targeted disruption of *Hmx2* in mice demonstrates the temporal and spatial involvement of *Hmx2* in the embryonic transition of the dorsal portion (pars superior) of the otocyst to a fully developed vestibular system. In *Hmx2* null embryos, a perturbation in cell fate determination in the lateral aspect of the otic epithelium results in reduced cell proliferation in epithelial cells, which includes the vestibular sensory patches and semicircular duct fusion plates, as well as in the adjacent mesenchyme. Consequently, enlargement and morphogenesis of the pars superior of the otocyst to form a complex labyrinth of cavities and ducts is blocked, as indicated by the lack of any distinguishable semicircular ducts, persistence of the primordial vestibular diverticula, significant loss in the three cristae and the macula utriculus, and a fused utriculosaccular chamber. The developmental regulators *Bmp4*, *Dlx5* and *Pax2* all play a critical role in inner ear ontogeny, and the expression of each of these genes is affected in the *Hmx2* null otocyst suggesting a complex regulatory role for *Hmx2* in this genetic cascade. Both *Hmx2* and *Hmx3* transcripts are coexpressed in the developing central nervous system including the neural tube and hypothalamus. A lack of defects in the CNS, coupled with the fact that not all of the *Hmx2*-positive regions in developing inner ear are impaired in the *Hmx2* null mice, suggest that *Hmx2* and *Hmx3* have both unique and overlapping functions during embryogenesis.

Key words: Homeobox gene, *Hmx*, Inner ear development, Semicircular ducts, Gene knockout, Mouse, Cell proliferation

INTRODUCTION

The vertebrate inner ear is derived from one of three pairs of sensory placodes located in the anterior embryonic ectoderm. The other two placodes located more rostrally will contribute to the development of the sensory organs for olfaction and vision. Induction of the otic placode takes place at the 3- to 6-somite stage in vertebrates, as characterized by the acquisition of competence by the surface ectoderm adjacent to the hindbrain, and subsequent thickening of the placodal ectoderm (Torres and Giraldez, 1998).

During development, the otic placode invaginates and pinches off from the surface ectoderm to form an ellipsoid-shaped vesicle termed the otic vesicle (Hilfer et al., 1989). During the closure of the otic vesicle, positional information is gradually acquired by different regions of the otic epithelium, as indicated by the regionally restricted expression of different combinations of inner ear marker genes. Axial specification in the inner ear for sensory organs happens earlier than that for nonsensory organs. Transplantation experiments performed in chick demonstrated that patterning of sensory organs along the anterior-posterior (AP) axis is fixed first, followed by specification of the dorsal-ventral (DV) axis. At the same time, nonsensory epithelial cells maintain a certain degree of plasticity, since they can be reprogrammed when placed in a new environment (Wu et al., 1998). Different regions of the otocyst possess distinct positional information and express unique combinations of inner ear marker genes, which in turn ultimately determines their specific identities (Fekete, 1996). Regions with different identities display distinct capabilities in cell differentiation, proliferation and programmed cell death, a prerequisite for the transformation from an otocyst to an elaborate three-dimensional labyrinth. Precise outgrowth and fusion of the otic epithelium are morphogenetic milestones in the maturation of the inner ear. In the mouse, around E9.5 the anlagen of the endolymphatic duct bulges from the dorsal portion of the otic vesicle and elongates dorsally to form a hollow tube, which enlarges at its distal end to form a sac. Meanwhile, the otic epithelium destined to give rise to the cochlea enlarges ventrally and finally develops into a coiled duct. Morphogenesis of the otocyst pars superior into a vestibule requires very sophisticated shape changes. Formation

of the semicircular ducts initiates from paired outpocketings of otic epithelium. In the central regions of these pockets, the two epithelial layers on the opposing walls first become thinner and then detach from the underlying mesenchyme. Afterwards, these two walls approach one another to form an extensive region termed the fusion plate. Epithelial cells meeting at the fusion plate will meld into a single layer, and subsequently disappear via a possible mechanism involving either programmed cell death or epithelium cell retraction, or both. The semicircular ducts and associated canals are formed by the interactions between the remaining otic epithelium and it's adjacent periotic mesenchyme (Fekete et al., 1997; Frenz and Van De Water, 1991; Lang et al., 2000; Martin and Swanson, 1993). Undoubtedly, a balance between cell proliferation and programmed cell death plays a critical role in this process. Previous work has confirmed the existence of several regions of programmed cell death in the developing inner ear, including the fusion plates of the semicircular canals, the ventromedial otic vesicle and the base of the endolymphatic sac. In the chick, the overexpression of inhibitors of normal programmed cell death, such as *bcl2*, block semicircular canal fusion (Fekete et al., 1997). It has been proposed that the driving force pushing the apposing walls inward to form the fusion plate is generated by the interaction between the otic epithelium and the surrounding mesenchyme. The analysis of the inner ears of *netrin 1* null mice support this mechanism (Salminen et al., 2000). netrin 1 appears to be involved in a signaling pathway regulating cell proliferation in the periotic mesenchyme. When netrin 1 production by the presumptive fusion plate was disrupted, reduced cell proliferation in the underlying mesenchyme resulted in severe defects in fusion plate formation and therefore semicircular duct morphogenesis.

In the mouse, by E14.5, the basic architecture of the membranous labyrinth of the inner ear has been fully established. From E14.5 through adult stages, maturation occurs and a functional inner ear emerges, with the vestibule and cochlea being responsible for the senses of balance and hearing, respectively. The identification of developmentally important genes expressed in the inner ear has been steadily increasing, and the function of certain of these genes has been determined (Represa et al., 2000). Antagonizing the normal *Bmp4* signaling pathway with *noggin* disrupts inner ear development and demonstrates that local signals in the otic epithelium are essential for the correct formation of the inner ear (Chang et al., 1999; Gerlach et al., 2000). Different members of the homeobox gene superfamily are involved in all steps of inner ear development ranging from otic placode induction to maturation of a fully functional inner ear. Recent progress in mouse molecular genetics has allowed us to acquire specific information regarding the developmental contribution of individual genes to inner ear development. Certain homeobox genes are involved in regional specification of the inner ear, and some of these genes determine the fate of cells in their restricted expression domains. For example, *Pax2* is predominately expressed in the ventral otic epithelium, and *Pax2* null inner ears lack an identifiable cochlea (Represa et al., 2000; Torres et al., 1996). In addition, expression of a functional *Dlx5* gene in the dorsal portion of the otic vesicle is required for proper morphogenesis of the semicircular canals (Acampora et al., 1999; Depew et al., 1999). Murine *Otx1*, an orthologue of the *Drosophila orthodenticle* gene, is expressed in the ventrolateral wall of the otocyst with a dorsal limit in the presumptive lateral semicircular canal. *Otx1*null inner ears show an absence of the lateral semicircular canals and a malformed cochlea (Acampora et al., 1996; Morsli et al., 1999). However, it is common for a homeobox gene family that has several members to exhibit similar or even identical expression profiles and to be functionally interchangeable in certain aspects (Greer et al., 2000). The Hmx homeobox genes belong to a distinct family, which is of ancient origin, and their existence has been reported in many species (Bober et al., 1994; Stadler et al., 1995; Stadler et al., 1992; Stadler and Solursh, 1994; Wang et al., 1990; Wang et al., 2000). Three members of the Hmx homeobox gene family, designated *Hmx1*, *Hmx2* and *Hmx3* have been identified in mouse (Wang et al., 2000; Yoshiura et al., 1998). Regions where *Hmx1* likely exerts its developmental function are neural crest derivatives including the dorsal root ganglion, cranial ganglia, branchial arches and in the developing neural retina. Unlike *Hmx1*, *Hmx2* and *Hmx3* are clustered together on the same chromosome and have nearly identical expression domains that include the inner ear, CNS and uterus. Defects caused by the inactivation of *Hmx3* have been reported for the inner ear and in female fertility (Hadrys et al., 1998; Wang et al., 1998). An absence of horizontal cristae, a fused utriculosaccular chamber, a significant loss of vestibular hair cells and perimplantation infertility have been observed, indicating unique functions for *Hmx3*. However, analysis of these defects also suggests that some aspects of *Hmx3* function might have been compensated for by its sibling *Hmx2*, since not all cells expressing *Hmx3* are affected in the *Hmx3* null mice. In this paper, we will present the defects exhibited by *Hmx2* null mice to reveal its unique developmental function.

MATERIALS AND METHODS

Targeting of the *Hmx2* locus and generation of the *Hmx2* heterozygous and homozygous null animals

Genomic cloning of the *Hmx2* gene has been reported previously (Wang et al., 2000). Plasmid pW64b was generated by inserting an 11 kb *Eco*RI genomic fragment spanning the *Hmx2* gene into the vector pTZ18R (US Biochemicals). The 5′ *Eco*RI site is located in the intragenic region between the *Hmx2* and *Hmx3* genes. The 3′ *Eco*RI site is derived from the polylinker of the lambda DashII phage vector. In this *Eco*RI fragment, there are two *Xho*I sites. One is located in the *Hmx2* homeobox and the other is 1.2 kb 3′ to the homeobox. pW64b was double digested with *Sal*I and *Xho*I and the 1.2 kb *Xho*I fragment was re-inserted into the *Sal*I and *Xho*I site of pW64b, leaving an unique *Xho*I site in the *Hmx2* homeobox. Finally, the *ires.lacZ.neo* cassette purified from p1099 (Wang et al., 1998) was inserted into the unique *Xho*I site in the *Hmx2* homeobox, resulting in the targeting vector pW78a (Fig. 1A). The transcriptional orientation of the *ires.lacZ.neo* cassette was verified by DNA sequencing. The targeting construct was linearized by *Eco*RI digestion for electroporation and ES cell transfection, screening for recombinant R1 ES clones, production of chimeric animals and testing of germline transmission were performed as previously described (Wang and Lufkin, 2000; Wang et al., 1998). Insertion of the *ires.lacZ.neo* cassette into the *Hmx2* locus introduces new *Cla*I and *Xba*I sites, and Southern blot analysis was performed on tissue samples to genotype embryos and pups carrying the inactivated

Hmx2 allele designated *Hmx2*^{lacZ}. RNAse protection was carried out essentially as previously described (Wang et al., 1998). 100 μg total RNA extracted from *Hmx2*^{lacZ}+/+, *Hmx2*^{lacZ}+/– and *Hmx2*^{lacZ}–/– was used for RNAse protection assays. A 242 bp DNA fragment was PCR-amplified using primers TL245 (5′ AGCGCCAAACCGGAGCGG 3′) and TL246 (5′ CCGACGC-GTGTGCCATGT 3′). This fragment contains the homeobox of *Hmx2* and spans the restriction site used for insertion of the *ires.lacZ.neo* cassette and was used to make ^{32}P-labeled anti-sense riboprobe. A 271 bp cDNA fragment from the mouse β-actin gene was used as the internal control for the quantity and quality of total RNA.

β-galactosidase staining of whole-mount embryos, preparation of inner ears for histology, RNA in situ hybridization and analysis of cell proliferation (BrdU labeling) and apoptosis (TUNEL)

Embryos between the ages of embryonic day (E) 8.5 and E18.5 were collected from mating between viable *Hmx2*^{lacZ}–/– males and *Hmx2*^{lacZ}+/– females. Staining for β-galactosidase was performed as previously described with a minor modification in that 1% sodium deoxycholate was added to the staining solution (Frasch et al., 1995). Embryos older than E16.5 were decalcified in PBS containing 10% EDTA and 2.5% polyvinylpyrrolidone before being embedded in paraffin wax, and then sectioned at 8 μm. For standard histology, mice

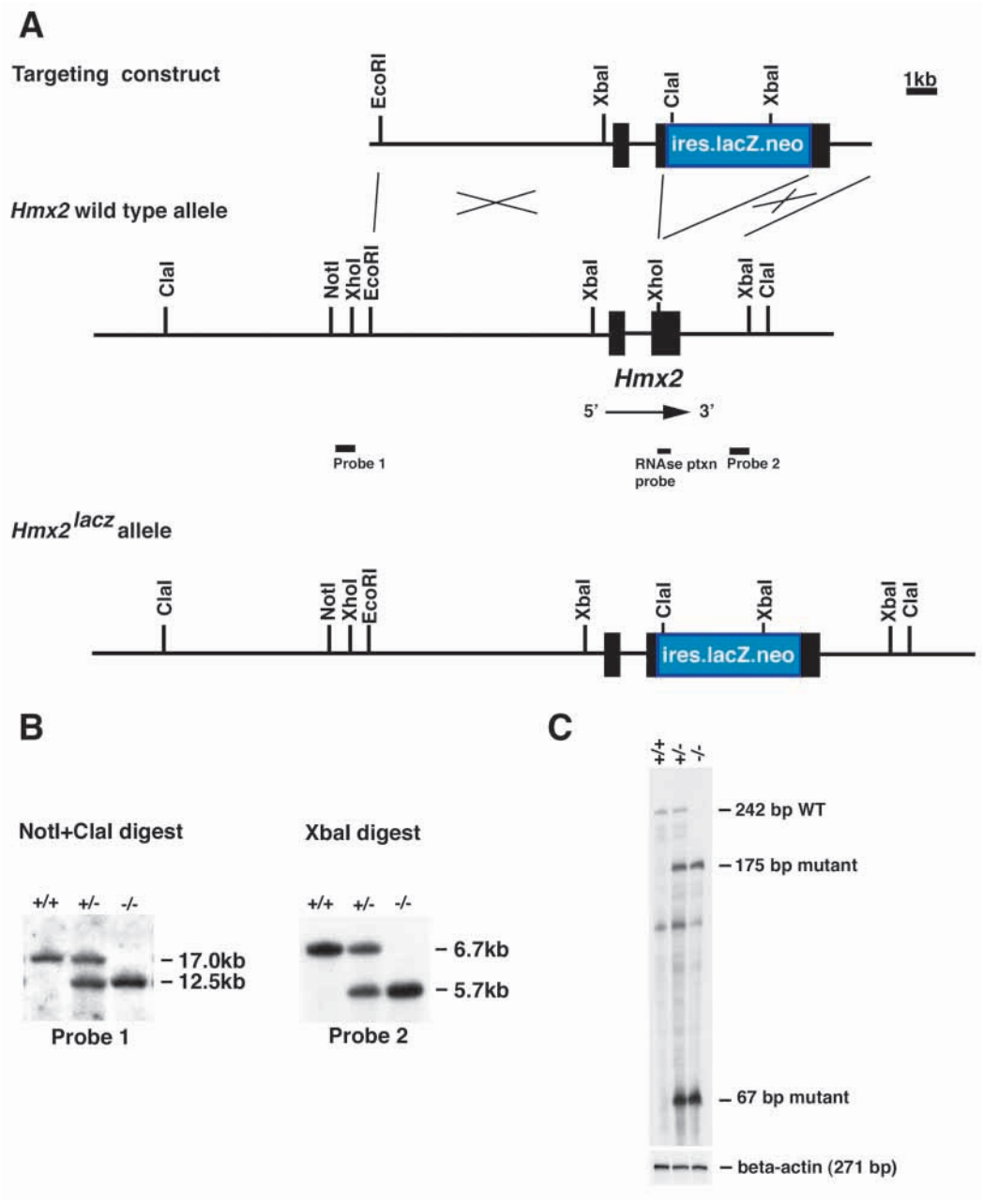

Fig. 1. Disruption of *Hmx2* by homologous recombination, mRNA analysis and genotyping of embryos carrying an *Hmx2*^{lacZ} mutant allele. (A) *Hmx2* wild-type locus, targeting construct and *Hmx2* mutant alleles. Homologous recombination of the targeting construct into the *Hmx2* locus results in the insertion of *ires.lacZ.neo* into the *Hmx2* homeobox. Owing to the presence of translation stop codons in all three open reading frames in the *ires.lacZ.neo* cassette, this mutant allele produces β-galactosidase and a nonfunctional truncated Hmx2 protein. The black boxes show the positions of the two *Hmx2* exons. The homeobox is located in the second exon. The transcriptional orientation of *Hmx2* is shown by an arrow. The positions and lengths of the probes used in Southern blot analysis and RNAse protection are also indicated by small black rectangles. (B) Southern blot assay from yolk sac DNA of wild-type, *Hmx2*^{lacZ}+/– and *Hmx2*^{lacZ}–/– embryos. Probe1 and Probe 2 are located outside of the targeting construct. Probe 1 detects a 17.0 kb wild-type *Not*I+*Cla*I fragment, as well as a 12.5 kb mutant *Not*I+*Cla*I band. Probe 2 hybridizes with a 5.7 kb mutant *Xba*I fragment instead of a 6.7 kb wild-type *Xba*I band because of the introduction of an additional *Xba*I by the *ires.lacZ.neo* cassette. Note: the *Xba*I site 5′ to the *Hmx2* gene is methylated in *dam*+ bacterial hosts. (C) RNAse protection analysis of *Hmx2* RNA expression in wild-type, *Hmx2*^{lacZ}+/– and *Hmx2*^{lacZ}–/– embryos. A 242 genomic fragment spanning the *Hmx2* homeobox was amplified by PCR using primers TL245 and TL246, and used as a template to prepare an antisense RNA riboprobe. RNA transcripts produced by the wild-type allele protect a fragment of 242 bp, whereas the *Hmx2* mutant transcripts protect two fragments of 175 bp and 67 bp.

were prepared by cardiac-perfusion with 4% paraformaldehyde, and inner ears were dissected, trimmed and fixed as previously described (Wang et al., 1998). Specimens were decalcified in 10% EDTA at 4°C for 5 days, dehydrated in ethanol, and treated in histoclear in preparation for embedding in paraffin wax. 7 μm microtome sections were cut, stained with Toludine Blue and mounted onto glass microscope slides in Permount for histological examination. Inner ears were obtained from embryos of E13.5, E14.5, E16.5 and E18.5. For each embryonic stage, three specimens were prepared from the *Hmx2*^{lacZ}+/– embryos (used as the controls) and three from the *Hmx2*^{lacZ}–/– embryos. In the E14.5-E18.5 specimens vestibular hair cells were identified and counted in the cristae of the semicircular ducts and the maculae of the utricle and saccule under a magnification factor of 400×. The total number of hair cells was counted in all three cristae, as well as in the superior and posterior cristae individually. Neurons of the spiral and vestibular ganglia were identified and counted under a magnification factor of 400×. Histological variables were analyzed for statistically significant differences between *Hmx2*^{lacZ}+/– and *Hmx2*^{lacZ}–/– at E14.5, E16.5 and E18.5, using the unpaired Student's *t*-test and the SigmaPlot computer program.

For the cell proliferation assay, pregnant mice were injected intraperitoneally with BrdU (50 μg/g body weight) at E10.5, E11.5 and E12.0. Embryos were collected 1 hour after injection and embryos processed as previously described (Tribioli and Lufkin, 1999; Wang and Lufkin, 2000). TUNEL was performed on paraffin sections as previously described (Tribioli and Lufkin, 1999; Wang and Lufkin, 2000; Wang et al., 1998). Embryos from E10.5 to E13.5 were collected. At least three control embryos (*Hmx2*^{lacZ}+/+ or *Hmx2*^{lacZ}+/–) and three *Hmx2*^{lacZ}–/– embryos at each embryonic stage were examined for both BrdU-labeling and TUNEL. Light micrographs were taken and the color was inverted using Adobe Photoshop 5.5.

^{35}S-labeled RNA in situ hybridization was performed as previously described (Tribioli and Lufkin, 1999; Wang and Lufkin, 2000; Wang et al., 1998) and embryos from E10.5 to E18.5 were collected. Comparable sections from at least three wild-type or *Hmx2*^{lacZ}–/– embryos of different stages were examined for each in situ probe. The in situ probe for *Hmx3* has been described previously (Wang et al., 1998). Other antisense probes used in this experiment were 1.2 kb *Bmp4*; 1.0 kb *Brain Factor 1*(*BF1*; now known as *Foxg1*); 400 bp *Dlx5*; 0.6 kb *Otx1*; 600 bp *netrin 1*; 500 bp *Pax2*; 1.0 kb *Sek1* (also known as *Epha4*). Wild-type and *Hmx2*^{lacZ}–/– embryos from E10.5 to E12.5 were isolated for whole-mount in situ hybridization. Preparation of antisense digoxiginin-labeled *Bmp4* RNA probe, hybridization and visualization of signals were performed essentially as previously described (Tribioli et al., 1997). Five embryos of the same genotype (+/+ or –/–) at different stages were pooled and probed with a dig-labeled *Bmp4* probe.

RESULTS

Hmx2 null mice display hyperactivity, head tilting and circling behavior

The function of *Hmx2* during early mouse embryonic development was examined by generating an *Hmx2* loss-of-function allele in mice (Fig. 1). Homologous recombination of the targeting construct into the chromosome leads to the insertion of the *ires.lacZ.neo* cassette into the DNA sequence encoding the third helix of the *Hmx2* homeodomain. Owing to the presence of translation stop codons in all three open reading frame in the *ires.lacZ.neo* cassette, this *Hmx2*^{lacZ}null allele will produce three protein products: (i) a truncated Hmx2 protein lacking the C-terminal portion of Hmx2 along with the third helix, the most critical DNA-binding portion of the homeodomain, (ii) β-galactosidase, and (iii) neomycin phosphotransferase. Five out of 96 G418-resistant ES clones tested had undergone a correct homologous recombination event. Two of the five clones, 4H5 and 4D3 were injected into blastocysts and the mutant allele was successfully transmitted through the germline.

Since no *Hmx2*-transcription control elements were deleted in the targeting strategy, integration of the *ires.lacZ.neo* reporter gene into *Hmx2* exonic sequences enables us to follow *Hmx2* gene expression by examining β-galactosidase activity. β-galactosidase expression of the *Hmx2*^{lacZ} heterozygotes faithfully reproduced *Hmx2* expression patterns as revealed by in situ hybridization on paraffin sections and in whole-mount embryos (Wang et al., 2000). Unlike *Hmx3*, *Hmx2* is still negative in the otic placode at E8.5 (Fig. 2A). *Hmx2* expression is first detectable at E9.0 and its expression becomes prominent from E9.5 onward in the anteriodorsal portion of the otic vesicle, as well as the cleft between the first and second branchial arches (Fig. 2B,C). In addition to its expression in the vestibular portion of the otic vesicle, from E12.0, *Hmx2* transcripts are strongly present in the central nervous system, including the developing neural tube, pons and hypothalamus. Its expression in the CNS is maintained at later stages (Fig. 2D and Fig. 3A,C). After E13.5, β-galactosidase activity from the *Hmx2*^{lacZ}+/– allele is detected in both the sensory and nonsensory epithelia of all three well-formed semicircular canals, endolymphatic sac, utricle and saccule (Fig. 3A,C,E). From E14.5, the stria vascularis of the cochlea begins to show β-galactosidase activity (Fig. 3C,E). *Hmx2*^{lacZ}+/– and wild-type mice are indistinguishable in their viability, behavior and fertility. Approximately 65% of the *Hmx2*^{lacZ}–/– mice in the outbred genetic background C57BL/6J×129X1/SvJ (previously 129/SvJ; Jackson Laboratory #000691) show classic vestibular defects as indicated by hyperactivity, head tilting and circling activity. The remaining *Hmx2*^{lacZ}–/– mice do not display any abnormalities in their behavior or fertility. Despite its strong expression in the central nervous system, loss of *Hmx2* was insufficient to cause any observable defect in the CNS as determined by the behavior, β-galactosidase activity and histological analysis of *Hmx2*^{lacZ}–/– mice and embryos (data not shown). Furthermore, RNA in situ hybridization with numerous probes corresponding to neurogenic developmental regulators from the paired, forkhead and homeodomain families (e.g. *Pax*, *Fox*, *Dlx*), as well as cell-cell signaling molecules of the *TGFβ* superfamily, failed to reveal any alterations in expression between wild-type and *Hmx2* ^{lacZ}–/– null embryos in the CNS (data not shown).

Structural abnormalities in the morphology and histology of *Hmx2* null inner ears

Multiple inner ear defects were evident in the *Hmx2*^{lacZ}–/– embryos following examination of whole-mount embryos and tissue sections stained for β-galactosidase activity. The most significant finding was a gross dysgenesis of all three semicircular ducts seen as early as E13.5 days in approximately 70% of the *Hmx2*^{lacZ}–/– embryos examined (compare Fig. 3B and 3A). The remaining 30% of the *Hmx2*^{lacZ}–/– embryos displayed variable defects in the vestibule between different individuals, and even between the membranous labyrinths of the same homozygous mouse embryos. At E18.5, in the most severe cases of malformation

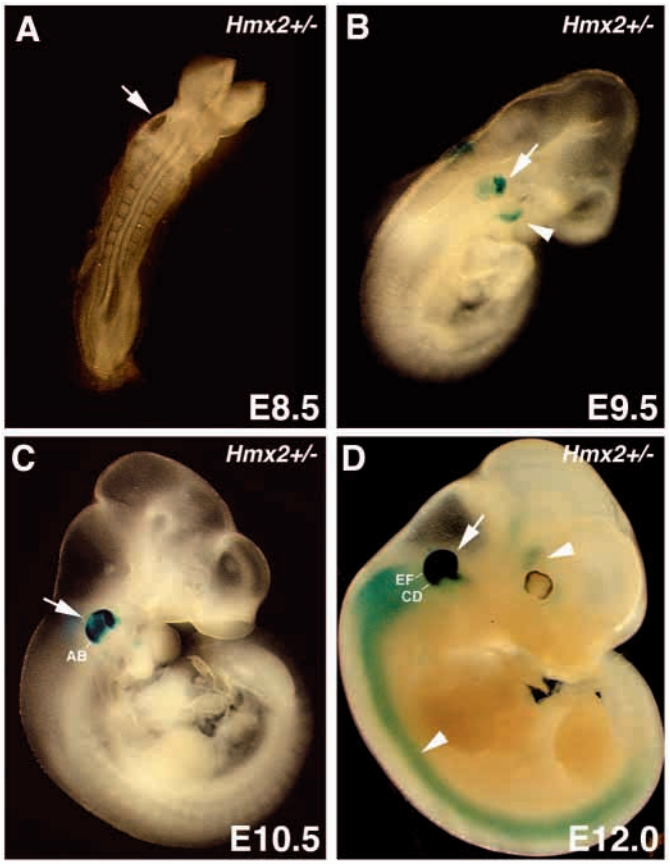

Fig. 2. Early embryonic expression pattern of *Hmx2* revealed by staining *Hmx2*^{lacZ}+/– whole mounts for β-galactosidase. Embryonic stages are indicated at the lower-right corner of each panel. β-galactosidase expression patterns are identical to that obtained by RNA in situ hybridization. (A) No β-galactosidase activity can be detected at E8.5. *Hmx2* is first turned on at E9.0. (B) At E9.5 and (C) E10.5, *Hmx2* expression becomes more prominent in the anterior portion of otic vesicle and otocyst, respectively and the cleft between the first and second branchial arches. (D) At E12.0, expression of *Hmx2* can also be seen in the developing neural tube and hypothalamus. Arrows indicate the positions of the otic anlagen. The arrowhead in B indicates the *Hmx2* expression in the cleft between the first and second branchial arches. Arrowheads in D indicate the *Hmx2* expression in the central nervous system. Letters AB, CD and EF indicate the level and orientation of corresponding sections shown in Fig. 6.

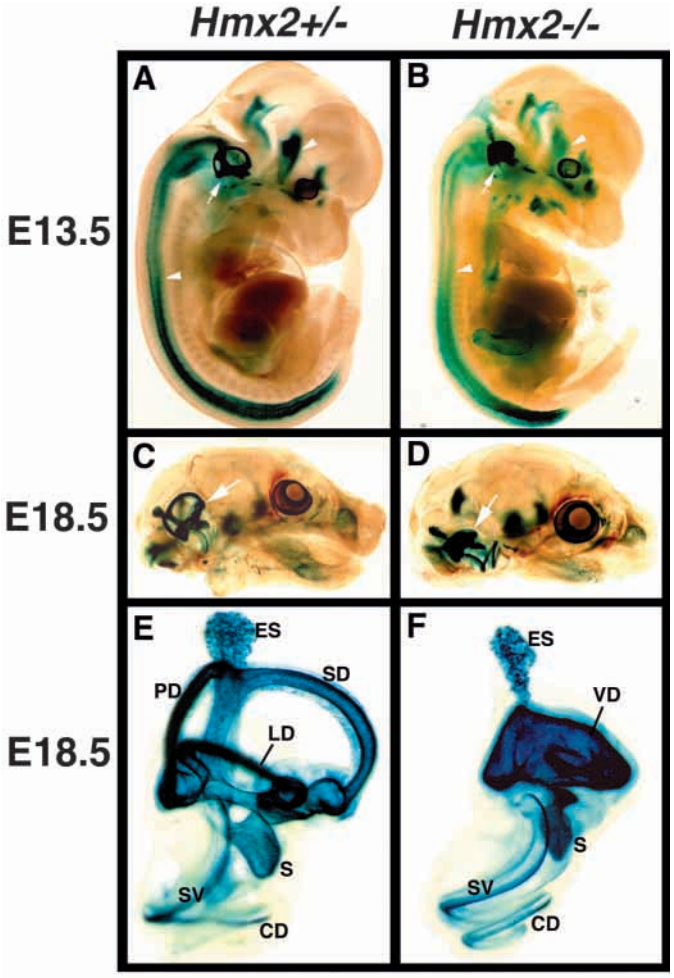

Fig. 3. Structural alteration of the *Hmx2*^{lacZ}null inner ears as shown by β-galactosidase activity in whole-mount embryos and dissected inner ears. The embryonic stages are indicated on the left. The genotype of each embryo is shown at the top. E and F are high power views of dissected *Hmx2*^{lacZ}+/– and *Hmx2*^{lacZ}–/– inner ears. Arrows in A-D indicate the positions of the inner ear. Arrowheads in panel A and B indicate *Hmx2*^{lacZ} expression in the developing neural tube and hypothalamus. In total, more than 20 embryos of each genotype from different embryonic stages were examined. CD, cochlear duct; ES, endolymphatic sac; LD, lateral semicircular duct; PD, posterior semicircular duct; S, saccule; SD, superior semicircular duct; SV, stria vascularis; VD, vestibular diverticulum.

of the vestibule, the *Hmx2*^{lacZ}–/– inner ears had only a primordial vestibular diverticula in place of well-developed semicircular ducts (compare Fig. 3D,F with C,E). The primordial vestibular diverticula persisted without the development of absorption foci (fusion plates) at the center of the diverticula until birth. Fig. 4 shows inner ears from E13.5 to E18.5 embryos clearly demonstrating the vestibular diverticula without any sign of apposition or fusion of the canal plate epithelia. At E18.5, the severity of the dysgenesis of the semicircular ducts increased, with less distinct folds representing the vestibular diverticula in these older specimens. In contrast, the development of the endolymphatic duct/sac and cochlear duct, appeared normal from the analysis of the both β-galactosidase stained specimens and tissue sections (Fig. 3 and Fig. 4, respectively).

Examination of the stained tissue sections also revealed the absence of semicircular duct formation as early as E13.5. As seen in Fig. 4A, control embryos at E13.5 show normal development of semicircular ducts as evident by two transected semicircular duct loops dorsal lateral to the utricle and saccule. At the same level, the *Hmx2*^{lacZ}–/– embryo has no semicircular ducts with only a rudimentary attempt at their formation as evident by the presence of two vestibular diverticulae and an absence of any transected loops (Fig. 4B). Fig. 4 also illustrates the fused utriculosaccular chamber in the *Hmx2*^{lacZ}–/– embryo, which was evident as early as E16.5. At E18.5 the same defects are still apparent with an increased severity in semicircular duct dysgenesis as well as enlargement of the fused common utriculosaccular chambers (Fig. 4E,F).

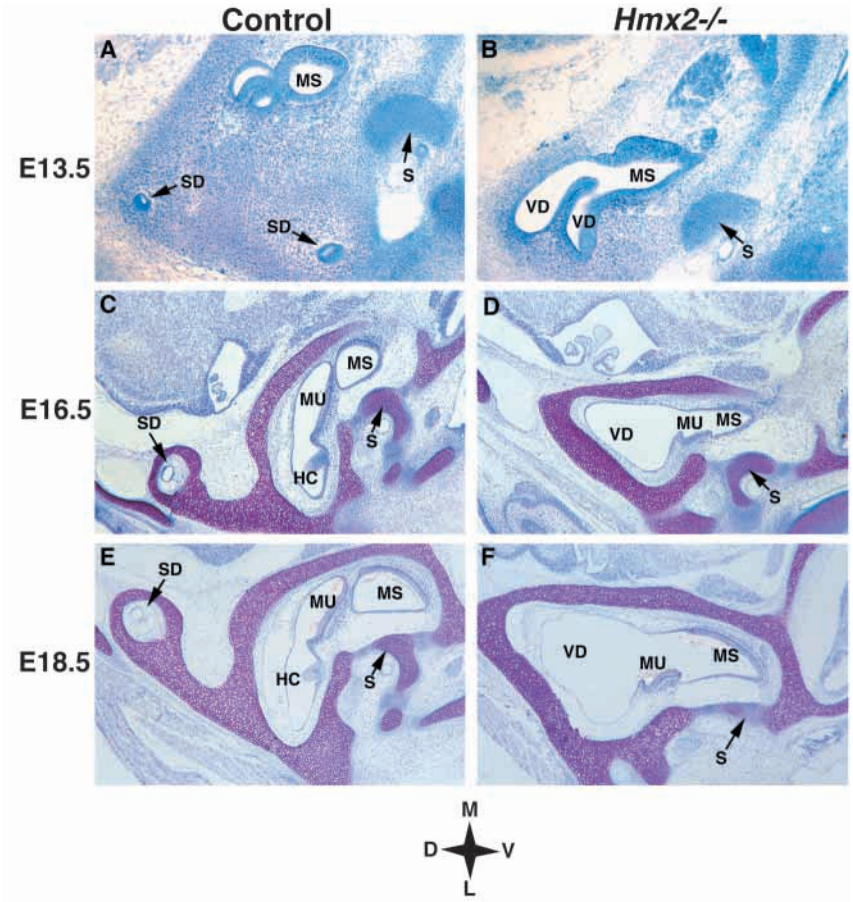

Fig. 4. Absence of semicircular duct formation **and** formation of a common macula in a fused utriculosaccular chamber in *Hmx2*^{lacZ} null mutants. (A) Section illustrating normal development of the semicircular ducts in the control embryo at E13.5. (B) *Hmx2*^{lacZ}*–/–* inner ear at E13.5 illustrating the formation of two vestibular diverticulae that are dorsal and lateral to a fused utriculosaccular chamber. (C) Control inner ear at E16.5 illustrating normally developed utricle and saccule chambers with associated maculae and horizontal ampulla. (D) *Hmx2*^{lacZ}*–/–* inner ear at E16.5 illustrating a common macula within a fused utriculosaccular chamber, lacking any distinction between the utricle and saccule other than the location of the maculae, as both appear to be combined ventrally. (E) Section illustrating normal development of the horizontal crista and ampulla coming off the utricular chamber in a control embryo at E18.5. (F) *Hmx2*^{lacZ}*–/–* inner ear at E18.5 demonstrating a more severe dysgenic vestibular system and increased fusion and enlargement of the common utriculosaccular chamber relative to earlier stages. D, dorsal; HC, horizontal crista; L, lateral; M, medial; MS, macula of saccule; MU, macula of utricle; S, footplate of the stapes; SD, semicircular duct; V, ventral; VD, vestibular diverticum.

In addition to a fused utriculosaccular chamber in the *Hmx2*^{lacZ}*–/–* embryos, a portion of this chamber had an area of a common macula, which was identifiable as early as E14.5 in the vestibule of the *Hmx2*^{lacZ}*–/–* embryos (data not shown). In other areas of the common cavity, sensory epithelium corresponding to the macula of the utricle was located on the lateral wall of the caudal utriculosaccular chamber where the utricle normally would be located (see Fig. 4). Accordingly, sensory epithelium corresponding to the macula of the saccule was also present in the *Hmx2*^{lacZ}*–/–* embryo, located on the medial wall of the rostral utriculosaccular chamber, which is where the saccule would normally be located (Fig. 4B,D,F). In contrast, the thickened sensory epithelia of the maculae fuse on the caudal aspect of the utriculosaccular chamber in the *Hmx2*^{lacZ}*–/–* embryos at E16.5 and persist until later stages (Fig. 4C,D). The posterior ampulla is present in *Hmx2*^{lacZ}*–/–* embryos along with the posterior crista ampullaris. A distinctly formed superior ampulla, however, is not present, although a patch of sensory epithelium that corresponds to the superior crista ampullaris can be identified in the area where the superior ampulla would normally be located (data not shown). Furthermore, the absence of the lateral crista and lack of a distinct lateral ampulla become evident as early as E14.5. In the *Hmx2*^{lacZ}*–/–* inner ear, the lateral crista ampullaris never forms and only a rudimentary attempt at formation of a lateral ampulla is evident off the vestibular diverticula, with a lack of any transected loops to provide evidence of developed semicircular ducts. The attempt at formation of a lateral ampulla may also simply be a transection through the lateral vestibular diverticulum, which is melding with the superior/posterior diverticulum as the *Hmx2*^{lacZ}*–/–* embryo develops in utero, further illustrating the increasingly severe lack of distinction in the vestibular diverticula as the mutants age.

Quantitative analysis of histological variables between control and *Hmx2*^{lacZ}*–/–* embryos

Progressive impairment of the sensory system of the inner ear was carefully examined during development. Statistically significant deficits in the total number of ampullary hair cells were found in the *Hmx2*^{lacZ}*–/–* embryos, with an 86% loss at E14.5, 64% at E16.5, and 68% at E18.5 (*P*-value=0.02, 0.0017 and 0.00056 respectively; Fig. 5A). Hair cell counts revealed statistically significant deficits in the number of utricular hair cells in the *Hmx2*^{lacZ}*–/–* embryos of 63% at E16.5 and 69% at E18.5 of 63% (*P*-value=0.006 and 0.0005 respectively; Fig. 5B). In contrast, saccular hair cell counts revealed no statistically significant differences between the controls and mutants at all embryonic ages examined (*P*-value=0.14, 0.25 and 0.58 at E14.5, E16.5 and E18.5 respectively; Fig. 5C).

Although the differences in the number of neurons at E14.5 and E16.5 were not significant, there was a progressive increase in the percentage loss in the number of vestibular ganglion neurons among the *Hmx2*^{lacZ}*–/–* embryos of 16% at E14.5, 31% at E16.5, and 51% at E18.5 (*P*=0.001; Fig. 5D). In contrast, there were no statistically significant differences between the controls and *Hmx2*^{lacZ}*–/–* embryos in the number of spiral ganglion neurons (*P*-value=0.1 at E14.5, 0.82 at E16.5, 0.38 at E18.5; Fig. 5E). Analysis of the number of hair cells in the superior ampulla showed statistically significant losses of 73% at E14.5, 52% at E16.5, and 61% at E18.5 in the *Hmx2*^{lacZ}*–/–* embryos (*P*-value=0.003, 0.01 and 0.0094; data not shown). The number of hair cells in the posterior ampulla also showed statistically significant deficits in the *Hmx2*^{lacZ}*–/–*

embryos of 69% at E14.5, 43% at E16.5, and 54% at E18.5 (*P*-value=0.00058, 0.00064, 0.013; data not shown). Histological measurements showed significant differences in the area of the utricular macula. Again, an increase in the percentage loss in the area of the utricular macula was evident: 50% at E14.5 (*P*-value=0.14), 75% at E16.5 (*P*-value=0.0014), and 54% at E18.5 (*P*-value=0.0005). In contrast, the area of the saccular macula did not show statistically significant deficits in the *Hmx2*^{lacZ}–/– embryos at E14.5 and E16.5, but did show a statistically significant loss at E18.5 of 32% (*P*-value=0.015). The total area of the cristae ampullaris showed statistically significant losses at all ages: 87% at E14.5, 43% at E16.5, and 30% at E18.5 (*P*-value=0.000076, 0.034, 0.0077 respectively). The measurement of the volume of the chambers constituting the *Hmx2*^{lacZ}–/– embryo inner ears revealed significant findings in the utricle, saccule, and the ampullae. The volume of the *Hmx2*^{lacZ}–/– utricle showed a significant deficit at E16.5 of 82% (*P*-value=0.0077). The measurement of the *Hmx2*^{lacZ}–/– saccular volume showed significant deficits of 82% at E14.5 (*P*-value=0.044), 53% at E16.5 (*P*-value=0.0024), and 59% at E18.5 (*P*-value=0.0051). Interestingly, the total volume measurement of the ampullae only showed a statistically significant deficit in the *Hmx2*^{lacZ}–/– embryos at E16.5 of 70% (*P*-value of 0.015).

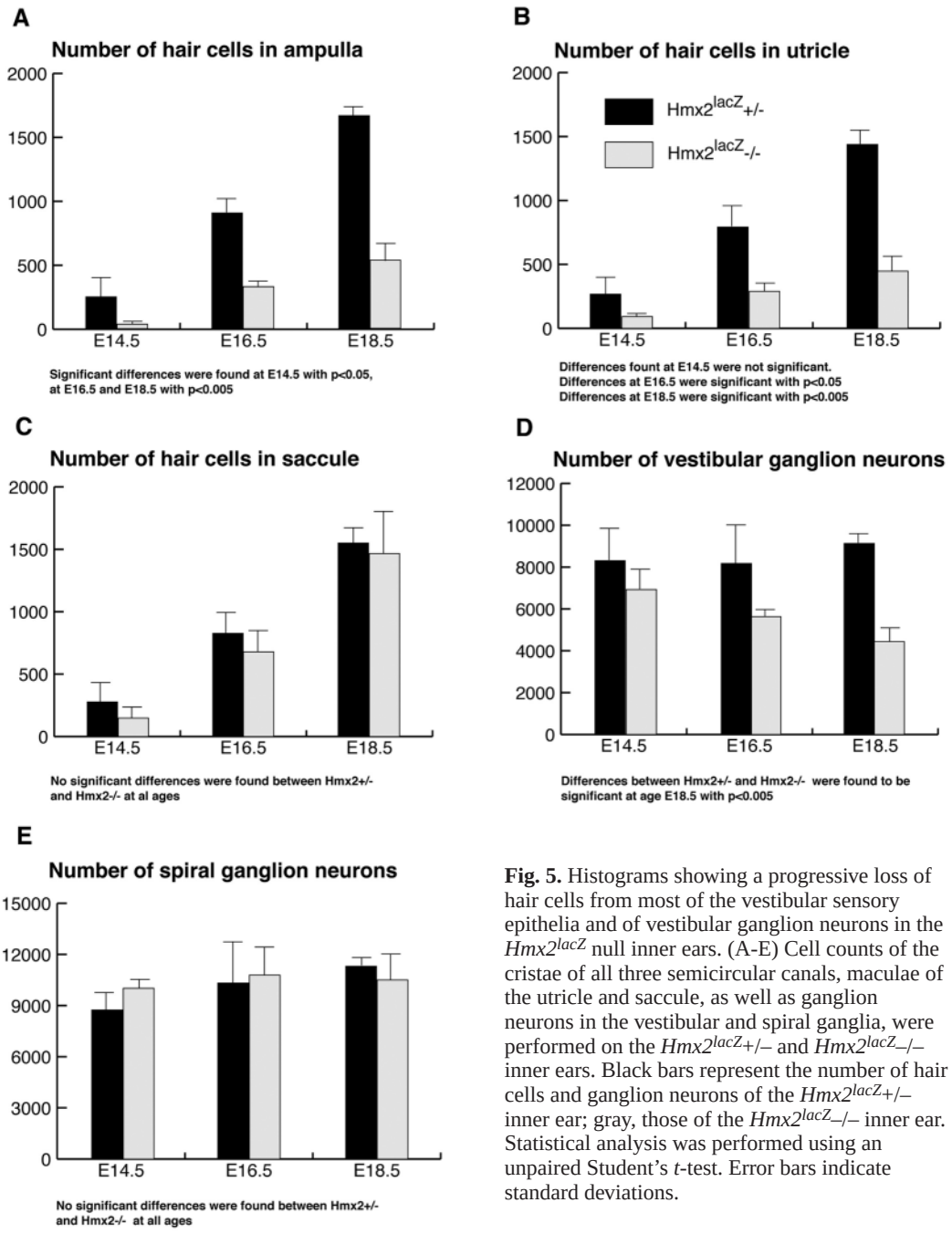

Fig. 5. Histograms showing a progressive loss of hair cells from most of the vestibular sensory epithelia and of vestibular ganglion neurons in the *Hmx2*^{lacZ} null inner ears. (A-E) Cell counts of the cristae of all three semicircular canals, maculae of the utricle and saccule, as well as ganglion neurons in the vestibular and spiral ganglia, were performed on the *Hmx2*^{lacZ}+/– and *Hmx2*^{lacZ}–/– inner ears. Black bars represent the number of hair cells and ganglion neurons of the *Hmx2*^{lacZ}+/– inner ear; gray, those of the *Hmx2*^{lacZ}–/– inner ear. Statistical analysis was performed using an unpaired Student's *t*-test. Error bars indicate standard deviations.

Reduced cell proliferation in the otic epithelium and the periotic mesenchymal cells in the *Hmx2*^{lacZ}null inner ears

Since gross morphogenetic abnormalities in the developing vestibular system can be observed as early as E13.5 (Fig. 3), molecular events mediating these defects must have occurred before this stage. Even though no gross morphological alterations can be detected between control and *Hmx2*^{lacZ}–/– whole-mount inner ears at E11.5, transverse sections through inner ears stained for β-galactosidase revealed clear differences in the epithelial invaginations between the *Hmx2*^{lacZ}+/– and *Hmx2*^{lacZ}–/– embryos (Fig. 6A and 6B). At this stage, *Hmx2* expression visualized by β-galactosidase activity is present in the entire dorsal otic vesicle excluding the otic epithelium cells destined to form the endolymphatic duct and sac (Fig. 6A). A small region of the lateral epithelium becomes thinner and the entire lateral aspect of the otic epithelium begins moving medially (arrow in Fig. 6A). In the *Hmx2*^{lacZ}–/– otic vesicle, neither the thinning nor the invagination of the lateral epithelium takes place (Fig. 6B) but instead, the thickness of the entire *Hmx2*^{lacZ}–/– otic epithelium remains uniform (Fig. 6B). In wild-type embryos

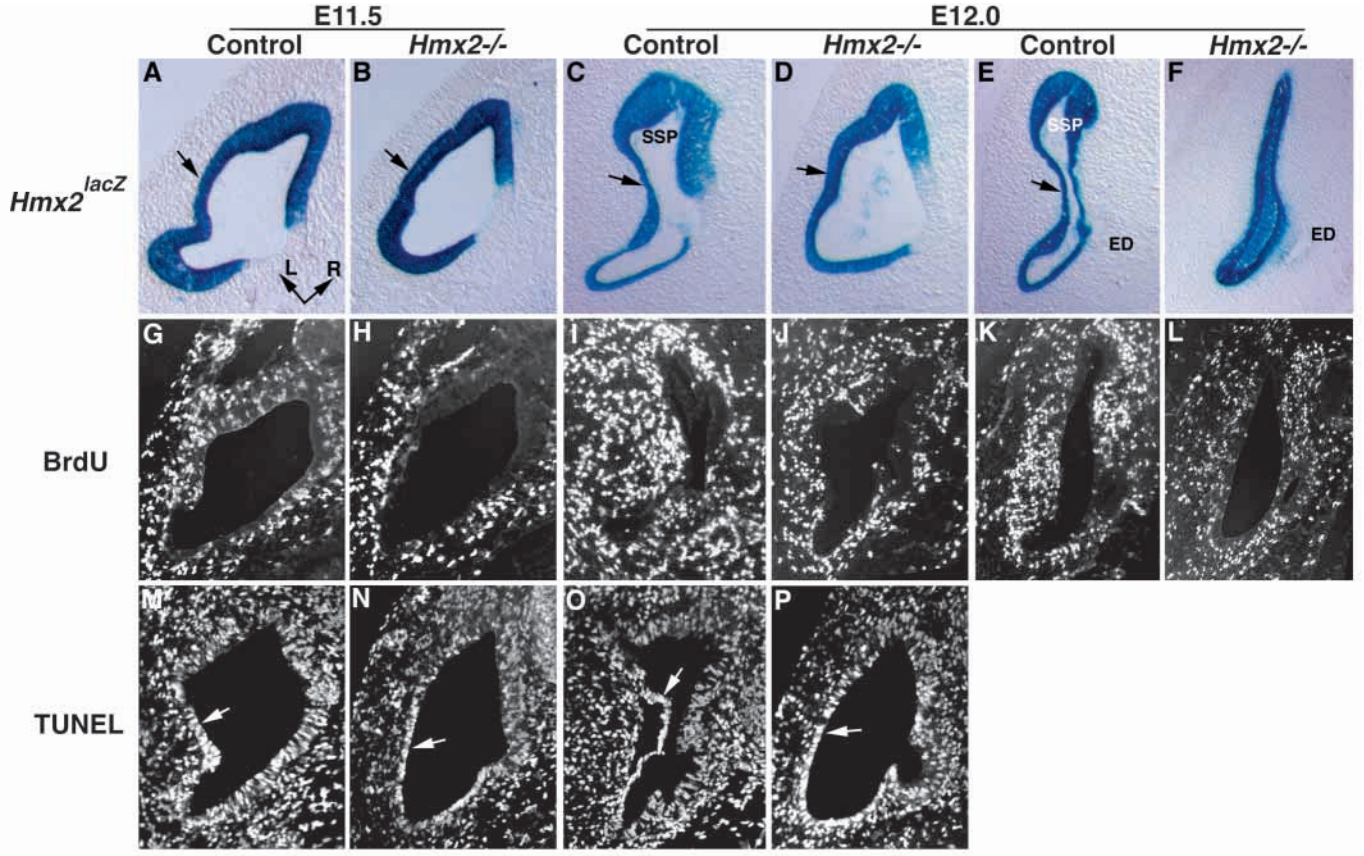

Fig. 6. Cell proliferation in the developing inner ear is affected by the loss of *Hmx2*. A-F show the morphological alteration of the $Hmx2^{lacZ}$–/– inner ear at E11.5 and E12.0 by examining β-galactosidase activity. Arrows indicate the presumptive fusion plate that is undergoing thinning and invagination. E and F are sections dorsal to C and D, respectively. The approximate level of sectioning is also indicated in Fig. 2. G-L are the comparable anti-BrdU-labeled sections showing the reduced rate of cell proliferation in the developing $Hmx2^{lacZ}$–/– inner ears. Genotypes and embryonic stages are indicated at the top of each column. Control corresponds to either $Hmx2^{lacZ}$+/+ or $Hmx2^{lacZ}$+/– genotypes. Overt morphological differences can be seen at E11.5 when the invagination of epithelial cells around the posterolateral boundary of the otic vesicle is delayed in the homozygotes (A and B). At E12.0, the close apposition of epithelial walls to form the fusion plates was not present in the otocyst of the $Hmx2^{lacZ}$–/– embryo (C,D,E,F). Both the epithelial cells and underlying periotic mesenchymal cells of the corresponding regions are undergoing reduced cell proliferation (J and L). M-P show the apoptotic activities of the otic epithelial cells in the control and $Hmx2^{lacZ}$–/– inner ears at E11.5 and E12.0. Arrows indicate the regions of the fusion plates. A higher percentage of cells in the fusion plates are undergoing programmed cell death relative to other regions in both control and $Hmx2^{lacZ}$–/– embryos. However, the $Hmx2^{lacZ}$–/– otic vesicles do not show an altered rate of cell death relative to the corresponding regions in the control embryos. L, lateral; R, rostral.

at E12.0, a thinned otic epithelial layer delaminates from the underlying mesenchyme and further moves toward the medial face, forming a structure termed the ‘fusion plate’ (arrows in Fig. 6C,E). Fig. 6E shows the fusion plate that has been pushed inward within close proximity of the medial face and is about to fuse into a single epithelial layer (which will eventually disperse) leaving behind an intact semicircular duct. However, in the $Hmx2^{lacZ}$–/– embryos, regional thinning and invagination of the lateral face of the otic epithelium towards the medial layer is not observed at this stage (Fig. 6D,F). Interestingly, at E13.5 when the 3-dimensional structure of the otic labyrinth has been well formed in the wild-type inner ear (Fig. 3A), the lateral epithelial layer of the $Hmx2^{lacZ}$–/– vestibular diverticulum begins to become thin and eventually detaches from the underlying mesenchyme (data not shown). However, the subsequent fusion plate process never occurs in the $Hmx2^{lacZ}$–/– inner ear, and this appears to be a principal reason for the failed vestibular morphogenesis in mice lacking *Hmx2*.

Our histological analysis has revealed that, in addition to gross morphological defects, $Hmx2^{lacZ}$–/– inner ears also display severe cell loss in both the sensory and nonsensory epithelia in the vestibular system. Cell proliferation and cell death both play critical roles in inner ear morphogenesis, and the spatial and temporal patterns of cell proliferation and cell death in the developing inner ear have been elaborately mapped (Fekete et al., 1997; Lang et al., 2000). The analysis of programmed cell death using the TUNEL assay was performed to examine cell death during inner ear morphogenesis on serial sections of wild-type and $Hmx2^{lacZ}$–/– embryos from E10.5 to E13.5. During the morphogenesis of the wild-type inner ear, the developing fusion plate is one of the ‘hot spots’ showing elevated apoptotic activities, which have been suggested to be critical in removing epithelial cells from the center of each canal and

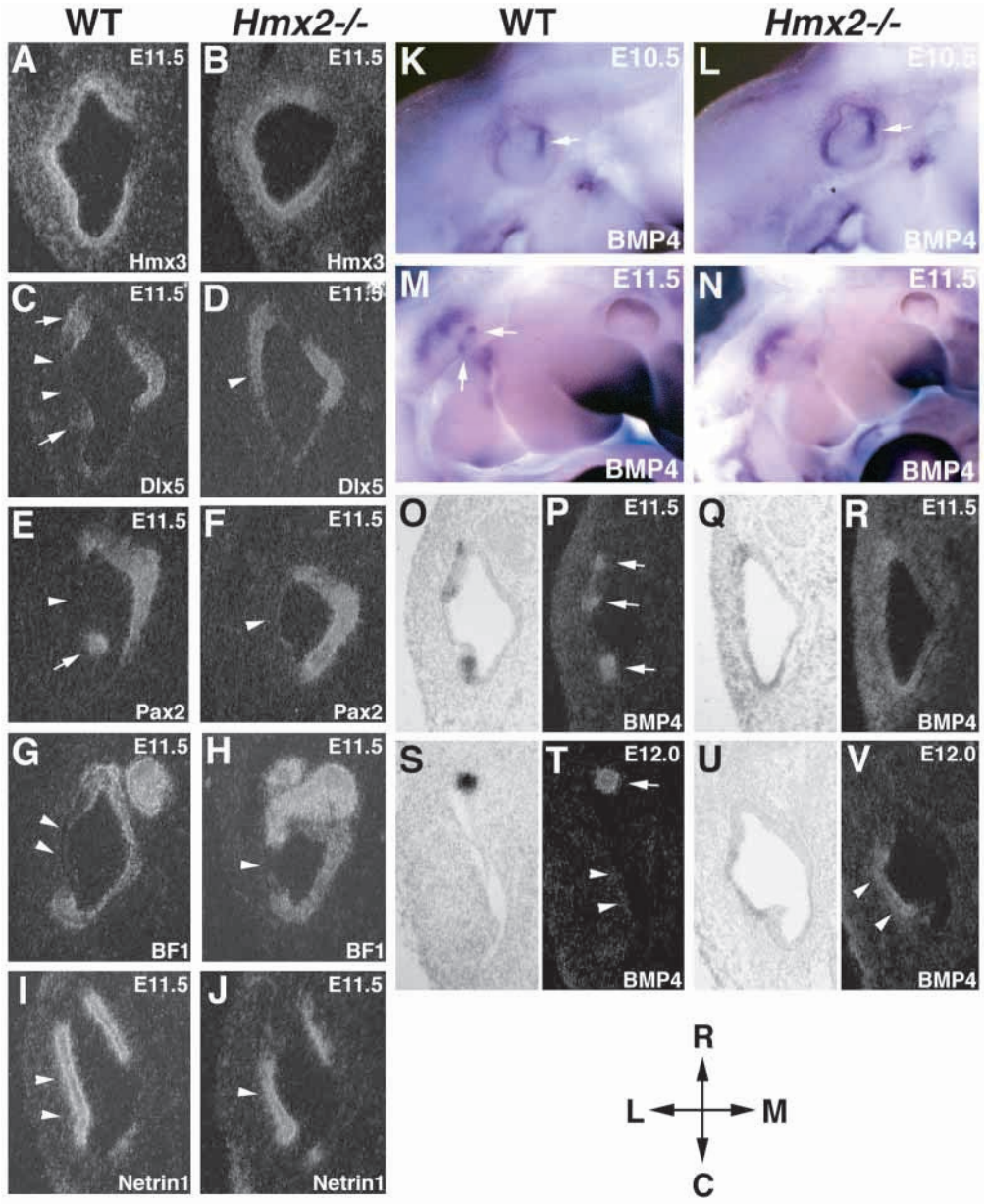

Fig. 7. Expression profile of developmental control genes in the otocysts of wild-type and *Hmx2*^{lacZ}null embryos. The *Hmx2* genotype is indicated on the top of each column. The molecular markers examined are listed on the lower right corner of each panel. The embryonic stages are indicated on the upper right corner of each panel. Arrows in K,L indicate the position of the developing sensory patches in the otic vesicle. Arrowheads indicate the presumptive fusion plate. (A,B) No discernible difference in *Hmx3* expression can be seen between wild-type and *Hmx2*^{lacZ}null backgrounds. (C,D) Altered *Dlx5* expression in the *Hmx2*^{lacZ}–/– inner ear is demonstrated by the loss of its expression in the discrete epithelial patches and ectopic *Dlx5* expression in the presumptive fusion plate. (E,F) Down regulation of *Pax2* expression in the lateral aspect of the *Hmx2*^{lacZ}null otocyst can be clearly seen at this stage. (G-J) Although both genes play a critical role in inner ear development, no discernible alteration of either *BF1* or netrin 1 expression was observed in the developing inner ears in the *Hmx2*^{lacZ}null embryos. At early embryonic stages, *Bmp4* mRNA is restricted to the sensory epithelial cells in the developing otic vesicle. K-N show the *Bmp4* expression in the otic vesicles in the wild-type and *Hmx2*^{lacZ}–/– embryos by whole mount in situ hybridization. (K,L) At E10.5, *Bmp4* is expressed in a correct spatial fashion in the *Hmx2*^{lacZ}–/– otocyst. No differences in *Bmp4* expression are seen at this stage of development. However, from E11.5, the sensory patches fail to express *Bmp4* (M,N). Instead, preferential expression of *Bmp4* in discrete regions of the lateral portion of the wild-type otic vesicle is replaced by a homogenous expression in the corresponding region in the *Hmx2*^{lacZ}null mutants (O,V). P, R, T and V show the expression pattern of *Bmp4* in the wild-type and *Hmx2*^{lacZ}–/– otic vesicles examined by in situ hybridization on paraffin sections of embryos of E11.5 and E12.0. O, Q, S and U are the corresponding bright-field views of P, R, T and V. C, caudal; L, lateral; M, medial; R, rostral.

finalizing the morphogenesis of the semicircular ducts. A higher percentage of cells in the prospective fusion plate do show apoptotic activities relative to other regions in the wild-type mouse otic vesicle (arrows in Fig. 6M,O). However, regions comparable with the presumptive fusion plate of the wild-type inner ear showed no alteration in apoptotic activities in the *Hmx2*^{lacZ}–/– otocyst (Fig. 6M and 6N; Fig. 6O and 6P). Similarly, in the other regions of the inner ear including the ventromedial otic vesicle, the base of the endolymphatic sac and the sensory organs, no significant difference in the rate of programmed cell death was observed in the *Hmx2*^{lacZ}–/– inner ears relative to wild-type embryos of the same stage. Thus changes in programmed cell death do not appear to play a prominent role in the mechanisms of *Hmx2*-mediated dysmorphogenesis.

However, when the BrdU incorporation rate was examined, reduced cell proliferation was observed in the *Hmx2*^{lacZ}–/– inner ears in both the otic epithelium and the periotic mesenchymal cells (Fig. 6G-L). In the wild-type otic vesicle at E11.5, epithelial cells, including the sensory and nonsensory epithelial cells show active cell proliferation (Fig. 6G and 6H), which was dramatically reduced in the *Hmx2*^{lacZ}–/– otic vesicle (Fig. 6G and 6H). In wild-type embryos at E12.0, when the fusion plate is being pushed toward the medial epithelial face, mesenchymal cells underlying the presumptive fusion plate as well as the recipient face of the medial epithelial layer display

elevated cell proliferation activity as indicated by the many BrdU-labeled cells (Fig. 6I,K). But in the *Hmx2*^{lacZ}–/– otic vesicle, less BrdU-positive cells were present in the corresponding regions and the distribution of proliferating cells was quite uniform throughout the periotic mesenchyme (Fig. 6J,L). Previous work has demonstrated that the periotic mesenchyme may provide the major driving force pushing the neighboring epithelial cells to undergo morphological changes (Salminen et al., 2000; Van De Water, 1983). Therefore, slowed cell proliferation exhibited by the otic epithelium and the surrounding periotic mesenchyme in the *Hmx2*^{lacZ}–/– inner ear may account, in part, for disruption of the morphogenesis of the vestibular system.

Inactivation of *Hmx2* affects the expression profile of developmental regulators that control inner ear ontogeny

Expression of genes with a demonstrated role in inner ear morphogenesis and differentiation was examined on paraffin sections and whole mounts of wild-type and *Hmx2*^{lacZ}–/– inner ears at embryonic stages preceding and coincident with the disruption in vestibular morphogenesis. At E10.5, all genes examined, including *BF1*, *Bmp4*, *Dlx5*, *Hmx3*, *netrin 1*, *Pax2*, *Otx1*and *Sek1*, showed no overt alteration in their expression in the *Hmx2*^{lacZ}–/– inner ear (Fig. 7K and 7L; data not shown). Homeobox genes *Hmx3* and *Otx1*, as well as the receptor tyrosine kinase gene *Sek1*, which all play a critical role in inner ear morphogenesis, do not show any altered expression patterns at any of the embryonic stages examined (Fig. 7A,B; and data not shown). Either the lack of a gene regulatory relationship between *Hmx2* and the above mentioned genes or the inability of *Hmx2* alone to alter the regulatory cascade may account for these findings. Owing to the severe morphological discrepancies between wild-type and *Hmx2*^{lacZ}–/– inner ears older than E13.5, altered expression of certain markers at later stages may be caused by indirect structural changes rather than direct regulatory effects. Thus in situ hybridization results on sections of embryos immediately preceding and coinciding with *Hmx2*^{lacZ}–/– inner ear dysmorphology (i.e. E11.5) are presented.

In wild-type embryos, the homeobox gene *Dlx5* is preferentially expressed in three different regions including the developing endolymphatic sac and epithelial patches which are located between the two *Bmp4*-positive spots (presumptive anterior and lateral cristae) in the anterior portion of the lateral aspect of the otic vesicle, as well as in the region anterior to *Bmp4*-positive sensory patch, in the posterior otic vesicle (arrows in Fig. 7C,P). Loss of *Dlx5* results in failed morphogenesis of the semicircular canals and failed cytodifferentiation within the vestibular epithelium (Acampora et al., 1999; Depew et al., 1999). In the *Hmx2*^{lacZ}–/– otic vesicle, the lateral gap between the rostral and caudal *Dlx5* expression domains was now filled with *Dlx5*-positive cells (arrowheads in Fig. 7C,D) suggesting either the derepression of *Dlx5* expression or the migration of *Dlx5*-positive cells into this region. *Pax2* is a paired-box containing transcription factor with a demonstrated role in patterning the inner ear. In addition to its expression in the medial epithelium of the dorsal otic vesicle, *Pax2* is also seen in restricted otic epithelial cells slightly anterior to the *Bmp4*-positive sensory patch in the posterior portion of the lateral layer (arrow in Fig. 7E). In the *Hmx2*–/– lateral otic epithelium, *Pax2* expression is diminished (Fig. 7E and 7F) indicating a requirement for *Hmx2* to maintain *Pax2* expression in these cells. At E10.5, *Bmp4* transcripts were present in a stripe of epithelial cells in the rostro-dorsal otic vesicle (arrow in Fig. 7K). At this stage, *Bmp4* mRNA can be detected in a correct spatial manner in the *Hmx2*^{lacZ}–/– inner ear (Fig. 7L). At E11.5, *Bmp4* transcripts mark presumptive sensory organs in the developing inner ear and were present primarily in two cell clusters at the anterior and posterior edges of the otic epithelium (arrows in Fig. 7M,P). These two discrete *Bmp4*-positive domains, which normally are separated by the region destined to form the fusion plate, will develop into cristae at later stages (Oh et al., 1996). Inactivation of *Hmx2* results in the disappearance of sensory patch-restricted *Bmp4* expression in the otic vesicle (Fig. 7N). In addition, *Bmp4* is upregulated and expressed uniformly in the lateral aspect of the otic epithelium including the presumptive fusion plates which are normally negative for *Bmp4* in wild-type inner ears (Fig. 7P,R), suggesting a role for *Hmx2* in repression of *Bmp4* in the cells constituting the future fusion plate. At E12.0 during fusion plate formation, *Bmp4* expression is strictly confined to the sensory organs (arrow in Fig. 7T) and is completely absent from the fusion plate in mouse (arrowheads in Fig. 7T). At this stage, ectopic presence of BMP4 in the fusion plate persists in the *Hmx2*^{lacZ}–/– otic vesicles (arrowheads in Fig. 7V).

In summary, loss of functional *Hmx2* leads to an alteration of the molecular identities of the cells in the dorsolateral aspect of the otic vesicle including the sensory cells and the prospective fusion plate. Taken together with the results from the cell proliferation assay, *Hmx2*^{lacZ}–/– fate-altered lateral epithelium acquired a reduced cell proliferation capability, which in turn impacted on the adjacent periotic mesenchyme, which normally does not express *Hmx2*. Hence changes in cell fate in restricted regions of the otic epithelium subsequently affects global morphogenesis of the entire vestibular system. In addition, the above RNA in situ data also indicate the existence of a genetic regulatory interaction between *Hmx2* and other inner ear developmental regulatory genes such as *Bmp4*, *Dlx5* and *Pax2*. Other factors showing restricted expression pattern in the inner ear were also investigated in the *Hmx2*^{lacZ}–/– embryos. Brain factor 1 (BF1), a winged helix transcription factor is confined to the epithelium on the medial aspect of the otic vesicle (Hebert and McConnell, 2000), however its absence in the dorsolateral face was maintained (Fig. 7G and 7H) in the *Hmx2*^{lacZ}–/– embryos. Likewise netrin 1, a member of the laminin-related secreted proteins, is expressed in the nonsensory epithelium known to form the fusion plate. Expression of *netrin 1* remains unchanged in the *Hmx2*^{lacZ}–/– embryos (Fig. 7I and 7J), indicating that inactivation of *Hmx2* alone is insufficient to affect *netrin 1* expression even though loss-of-function alleles for these two genes present a similar phenotypic mechanism affecting inner ear morphogenesis.

DISCUSSION

The role of *Hmx2* in murine inner ear development

Temporally, *Hmx2* expression exhibits a multi-phasic pattern in the developing inner ear. At the early otic vesicle stage (E9.5) *Hmx2* is strongly expressed in the anterior aspect of the vesicle. By E10.5 the strongest expression is in the

anterodorsal portion of the otocyst and at E12.5 the entire dorsal portion (pars superior) of the otocyst strongly expresses this gene. The areas of otic epithelium that express *Hmx2* include areas that will form both sensory and nonsensory epithelium and exclude those cells that form the future endolymphatic duct and sac. Its expression in the dorsal endolymphatic duct becomes prominent at E12.5 after the overall structure has already been established. Its late onset of expression, together with the unaffected expression of early inner ear markers in the *Hmx2*^{lacZ}–/– otocyst, indicate that *Hmx2* is unlikely to be involved in the induction of the otic placode or the initial morphogenesis of the otic vesicle. An in vitro fate map study of the murine otocyst (E11-E12.5) has determined that the pars superior portion of the otocyst participates in the formation of all the vestibular sensory receptors and generates all three of the semicircular ducts (Li et al., 1978). The functional data presented in this paper clearly demonstrate that *Hmx2* participates in the transformation of the pars superior of the otic vesicle into a complex mature vestibular labyrinth. Defects resulting from the absence of *Hmx2* includes the lack of any distinguishable semicircular ducts, persistence of the primordial vestibular diverticula, a fused utriculosaccular space in which a common macula is formed, as well as a severe loss of epithelial cells (both sensory and nonsensory) in the developing vestibule, clearly indicating a severe disruption of inner ear development. During the morphogenesis of complex organs, the production of cells and the fusion of tissue layers at specific regions are critical events. Within the inner ear, cell proliferation provides both material and a mechanical driving force for epithelial fusion initiated at the fusion plate, the elaboration of which will ultimately finalize the basic architecture of the vestibular system. At E11.5 in the *Hmx2*^{lacZ}–/– otocyst, a reduced rate of cell division was observed in the otic epithelium where *Hmx2* is normally expressed, as well as in the adjacent periotic mesenchyme. At the same stage, thinning of the epithelial layer in specific regions of the otic vesicle fails to take place, suggesting that at this stage no region in the *Hmx2*^{lacZ}–/– otocyst has become competent to form a fusion plate. However, the finding of a thinned epithelial layer and its detachment from the underlying basement membrane at E13.5 suggest a potential delayed initiation of fusion plate formation. However, the eventual fusion of the apposing walls of the otocyst to form a semicircular duct never takes place. During the transformation from an otic vesicle to an otic labyrinth, morphogenetic milestones such as the thinning of the epithelial layer, loss of epithelial morphology, detachment from the basement membrane and fusion of the apposing epithelial walls, are strictly coordinated in a temporal and spatial manner (Martin and Swanson, 1993). The delayed initiation of fusion plate formation in the *Hmx2*^{lacZ}–/– inner ear may miss the time window when the otic vesicle and surrounding environment are competent to carry out the fusion process.

Molecules from different gene families have been shown to play a critical role in epithelial fusion. One well-characterized molecule is the laminin-like protein, netrin 1. In addition to its function in axon guidance and cell migration in the central nervous system, netrin 1 is also required for fusion plate formation during inner ear morphogenesis (Salminen et al., 2000). Laminins are a major component of the ECM and previous work has shown that remodeling of the extracellular matrix (ECM) in the basement membrane is a key event in axonal guidance, cell migration, angiogenesis and morphogenesis of complex organs. It had been proposed that the robust presence of netrin 1 in the fusion plate might either compete with other laminin molecules to disrupt the laminin network in the basement membrane, or upregulate the production of matrix metalloproteinases to remodel the ECM network. In the netrin 1 null otocyst, the epithelial wall of the presumptive fusion plate became thinner. However, these thinned layers failed to change their epithelial morphology and subsequently detach from the underlying basement membrane. The strong expression of *netrin 1* in the *Hmx2*^{lacZ}–/– inner ears at all stages suggests that netrin 1 alone is insufficient for the formation of the fusion plate. It is possible that the prospective epithelium has to first become competent so that it can be responsive to netrin 1. In this respect, *Hmx2* may be needed to determine the fate of epithelial cells in specific regions of the otocyst. The reduced cell proliferation rate observed in the *Hmx2*^{lacZ}–/– periotic mesenchymal cells further suggests that *Hmx2* and netrin 1 may work cooperatively to control fusion plate formation by affecting cell proliferation of the neighboring mesenchyme. Also, the entry points when the two genes exert their functions are different since *Hmx2* clearly functions at an earlier stage than *netrin 1*. Based upon our in situ hybridization data, although these two genes share many overlapping expression domains, a clear regulatory interaction cannot be established between *Hmx2* and *netrin 1*. There are two possibile mechanisms to account for this. First, both genes may use independent pathways to regulate cell proliferation. Second, there is a regulatory interaction existing between these two genes, however, inactivation of *Hmx2* alone is insufficient to alter *netrin 1* expression, as other genes might compensate for the function of *Hmx2*. One such candidate is *Hmx3*, however, the persistence of netrin 1 in the developing *Hmx3* null inner ear suggests either a possible functional redundancy between *Hmx2* and *Hmx3* in regulating *netrin 1* (Salminen et al., 2000), or no regulatory interaction. The assessment of an overlapping role of *Hmx2* and *Hmx3* in controlling *netrin 1* (and other inner ear-specific genes) will be obtained from the analysis of embryos carrying combined loss-of-function alleles for *Hmx2* and *Hmx3*. Interestingly, certain phenotypic aspects of a previously generated *Hmx3-PGKneo* null allele share some overlap with the *Hmx2* phenotype described here (Hadrys et al., 1998). However, this overlap was not observed in mice carrying either of two independent *Hmx3* null alleles that lacked PGKneo and which were additionally shown to have no affect on the expression of the neighboring *Hmx2* gene (Wang et al., 1998). As PGKneo is notorious for affecting adjacent gene expression within tens of kilobases (Olson et al., 1996), a plausible explanation for the partial phenotypic overlap is that the previously described *Hmx3-PGKneo* allele (Hadrys et al., 1998) is also affecting, in a negative manner, the expression of the closely linked *Hmx2* gene.

Differential expression of varied combinations of developmental patterning genes gives distinct molecular identities to different cell populations, which consequently display unique capabilities in cell proliferation, apoptotic activity and responsiveness to the environment (Fekete, 1996). In the *Hmx2*^{lacZ}–/– otocyst, cells in a subset of the *Hmx2*-expressing domains have changed their fate as indicated by the altered expression of specific inner ear markers. The loss of

expression in the presumptive sensory epithelium of *Bmp4*, *Dlx5* and *Pax2*, together with ectopic activation of *Bmp4* and *Dlx5* in the prospective fusion plate, indicate a substantial alteration in cell fate in the otic epithelium of the pars superior. As a result of this cell fate alteration, the otic epithelium fails to communicate properly with the periotic mesenchyme, and in return, proper inner ear morphogenesis is severely impaired (Van De Water, 1983). Here we show that *Hmx2*, a homeodomain transcription factor affects the rate of cell proliferation of the otic epithelium, as well as the neighboring mesenchymal tissue. The identification of cell-cell signaling factors bridging the gap between the different tissues will be important. In this study, it is interesting that BMP4, a putative crista marker was present at E10.5, but disappeared by E11.5, suggesting that the cristae might be specified initially but fail to develop properly in the absence of *Hmx2*.

In summary, a normal function of *Hmx2* is to govern the specification and commitment of epithelial cells in the pars superior portion of the otocyst to undergo the proliferative growth and fusion processes to form a mature and functional vestibular system.

Functional relationship between *Hmx2* and *Hmx3* in mouse development

Hmx2 and *Hmx3* are an ideal pair of homeobox genes to investigate functional redundancy existing between members of the same gene family. The highly similar expression patterns and close linkage on chromosome 7 suggest that these two genes may share certain of the same transcriptional regulatory elements during mouse development and the similarity in the DNA-binding homeodomain suggest that these two genes may share many downstream regulatory targets. In the central nervous system and uterus, *Hmx2* and *Hmx3* show identical expression profiles (Wang et al., 2000; Wang et al., 1998), but in the *Hmx2*^{lacZ}–/– animals, no obvious defect was detected in either of these tissues. By comparing the defects in the individual *Hmx2* and *Hmx3* null inner ears, the unique developmental function of each of these genes can be identified. In the *Hmx3* null inner ear, the gross structure of the three semicircular canals forms except the horizontal ampulla and its associated crista are absent. In the ventral part of the vestibule, the utricle and saccule are fused into one chamber in which a significant cell loss occurs in both sensory maculae. This indicates that *Hmx3* alone uses a different mechanism to effect cell fate determination than by facilitating fusion plate formation and subsequent closure of the semicircular ducts. Disruption of *Hmx2*, despite its later onset of expression, results in a more severe inner ear phenotype than loss of *Hmx3*. In the *Hmx2*^{lacZ}–/– inner ear, anterior and dorsal regions along the corresponding AP and DV axes of the developing vestibule are more severely affected than in *Hmx3* null mice. Even though *Hmx2* and *Hmx3* are both involved in cell fate determination in specific regions of the otic epithelium, the consequences are different. Loss of *Hmx3* primarily influences the development of a subset of sensory receptor cells, but not the overall morphogenesis of the inner ear. In contrast, *Hmx2* is not only involved in cell fate determination of vestibular sensory areas, but also the morphological transformation mediated by the nonsensory epithelial cells. Even though *Hmx3* is transcriptionally activated about 8 hours earlier in the otic placode, the time point when *Hmx3* exerts its function seems to be later than that of *Hmx2*. Moreover, inactivation of *Hmx3* generates a milder phenotype, as fewer structures and tissue types are affected. It is also notable that some regions coexpressing *Hmx2* and *Hmx3*, such as the saccule, posterior ampulla and endolymphatic duct are not severely affected in either mutant. One explanation is that *Hmx2* and *Hmx3* may share redundant functions during inner ear and CNS development or they may be expressed in tissues where they exert no developmental function, possibly owing to a lack of a necessary cofactor(s). The unique and overlapping functions of each gene will be more clearly understood by comparing the inner ear phenotypes of mice carrying individual as well as a combined mutation in *Hmx2* and *Hmx3*.

The authors gratefully acknowledge Yan-Jie Chang, Jingxian Liu, Wei Liu, Dilip Madnani, Steve Raft and Cynthia Shoemaker for their technical assistance. We would like to thank Peter Gruss and Brigid Hogan for providing RNA in situ probes.

REFERENCES

Acampora, D., Mazan, S., Avantaggiato, V., Barone, P., Tuorto, F., Lallemand, Y., Brulet, P. and Simeone, A. (1996). Epilepsy and brain abnormalities in mice lacking the *Otx1* gene. *Nat. Genet.* **14**, 218-222.

Acampora, D., Merlo, G. R., Paleari, L., Zerega, B., Postiglione, M. P., Mantero, S., Bober, E., Barbieri, O., Simeone, A. and Levi, G. (1999). Craniofacial, vestibular and bone defects in mice lacking the *Distal-less*-related gene *Dlx5*. *Development* **126**, 3795-3809.

Bober, E., Baum, C., Braun, T. and Arnold, H. H. (1994). A novel *NK*-related mouse homeobox gene: expression in central and peripheral nervous structures during embryonic development. *Dev. Biol.* **162**, 288-303.

Chang, W., Nunes, F. D., De Jesus-Escobar, J. M., Harland, R. and Wu, D. K. (1999). Ectopic noggin blocks sensory and nonsensory organ morphogenesis in the chicken inner ear. *Dev. Biol.* **216**, 369-381.

Depew, M. J., Liu, J. K., Long, J. E., Presley, R., Meneses, J. J., Pedersen, R. A. and Rubenstein, J. L. (1999). Dlx5 regulates regional development of the branchial arches and sensory capsules. *Development* **126**, 3831-3846.

Fekete, D. M. (1996). Cell fate specification in the inner ear. *Current Opin. Neurobiol.* **6**, 533-541.

Fekete, D. M., Homburger, S. A., Waring, M. T., Riedl, A. E. and Garcia, L. F. (1997). Involvement of programmed cell death in morphogenesis of the vertebrate inner ear. *Development* **124**, 2451-2461.

Frasch, M., Chen, X. and Lufkin, T. (1995). Evolutionary-conserved enhancers direct region-specific expression of the murine *Hoxa-1* and *Hoxa-2* loci in both mice and *Drosophila*. *Development* **121**, 957-974.

Frenz, D. A. and Van De Water, T. R. (1991). Epithelial control of periotic mesenchyme chondrogenesis. *Dev. Biol.* **144**, 38-46.

Gerlach, L. M., Hutson, M. R., Germiller, J. A., Nguyen-Luu, D., Victor, J. C. and Barald, K. F. (2000). Addition of the BMP4 antagonist, noggin, disrupts avian inner ear development. *Development* **127**, 45-54.

Greer, J. M., Puetz, J., Thomas, K. R. and Capecchi, M. R. (2000). Maintenance of functional equivalence during paralogous Hox gene evolution. *Nature* **403**, 661-665.

Hadrys, T., Braun, T., Rinkwitz-Brandt, S., Arnold, H. H. and Bober, E. (1998). Nkx5-1 controls semicircular canal formation in the mouse inner ear. *Development* **125**, 33-39.

Hebert, J. M. and McConnell, S. K. (2000). Targeting of cre to the Foxg1 (BF-1) locus mediates loxP recombination in the telencephalon and other developing head structures. *Dev. Biol.* **222**, 296-306.

Hilfer, S. R., Esteves, R. A. and Sanzo, J. F. (1989). Invagination of the otic placode: normal development and experimental manipulation. *J. Exp. Zool.* **251**, 253-264.

Lang, H., Bever, M. M. and Fekete, D. M. (2000). Cell proliferation and cell death in the developing chick inner ear: spatial and temporal patterns. *J. Comp. Neurol.* **417**, 205-220.

Li, C. W., Van De Water, T. R. and Ruben, R. J. (1978). The fate mapping of the eleventh and twelfth day mouse otocyst: an in vitro study of the sites of origin of the embryonic inner ear sensory structures. *J. Morphol.* **157**, 249-267.

Martin, P. and Swanson, G. J. (1993). Descriptive and experimental analysis of the epithelial remodellings that control semicircular canal formation in the developing mouse inner ear. *Dev. Biol.* **159**, 549-558.

Morsli, H., Tuorto, F., Choo, D., Postiglione, M. P., Simeone, A. and Wu, D. K. (1999). Otx1 and Otx2 activities are required for the normal development of the mouse inner ear. *Development* **126**, 2335-2343.

Oh, S. H., Johnson, R. and Wu, D. K. (1996). Differential expression of bone morphogenetic proteins in the developing vestibular and auditory sensory organs. *J. Neurosci.* **16**, 6463-6475.

Olson, E. N., Arnold, H. H., Rigby, P. W. and Wold, B. J. (1996). Know your neighbors: three phenotypes in null mutants of the myogenic bHLH gene *MRF4*. *Cell* **85**, 1-4.

Represa, J., Frenz, D. A. and Van De Water, T. R. (2000). Genetic patterning of embryonic inner ear development. *Acta Otolaryngol.* **120**, 5-10.

Salminen, M., Meyer, B. I., Bober, E. and Gruss, P. (2000). netrin 1 is required for semicircular canal formation in the mouse inner ear. *Development* **127**, 13-22.

Stadler, H. S., Murray, J. C., Leysens, N. J., Goodfellow, P. J. and Solursh, M. (1995). Phylogenetic conservation and physical mapping of members of the *H6* homeobox gene family. *Mamm. Genome* **6**, 383-388.

Stadler, H. S. and Solursh, M. (1994). Characterization of the homeobox-containing gene *GH6* identifies novel regions of homeobox gene expression in the developing chick embryo. *Dev. Biol.* **161**, 251-262.

Stadler, H. S., Padanilam, B. J., Buetow, K., Murray, J. C. and Solursh, M. (1992). Identification and genetic mapping of a homeobox gene to the 4p16.1 region of human chromosome 4. *Proc. Natl. Acad. Sci. USA* **89**, 11579-11583.

Torres, M. and Giraldez, F. (1998). The development of the vertebrate inner ear. *Mech. Dev.* **71**, 5-21.

Torres, N., Gomezpardo, E. and Gruss, P. (1996). Pax2 contributes to inner ear patterning and optic nerve trajectory. *Development* **122**, 3381-3391.

Tribioli, C., Frasch, M. and Lufkin, T. (1997). *Bapx1:* an evolutionary-conserved homologue of the *Drosophila bagpipe* homeobox gene is expressed in splanchnic mesoderm and the embryonic skeleton. *Mech. Dev.* **65**, 145-162.

Tribioli, C. and Lufkin, T. (1999). The murine *Bapx1* homeobox gene plays a critical role in embryonic development of the axial skeleton and spleen. *Development* **126**, 5699-5711.

Van De Water, T. R. (1983). Embryogenesis of the inner ear: In vitro studies. In *Development of the Auditory and Vestibular Systems* (ed. R. Romand), pp. 337-372. New York: Academic Press.

Wang, G. V., Dolecki, G. J., Carlos, R. and Humphreys, T. (1990). Characterization and expression of two sea urchin homeobox gene sequences. *Dev. Genet.* **11**, 77-87.

Wang, W., Lo, P., Frasch, M. and Lufkin, T. (2000). *Hmx*: an evolutionary conserved homeobox gene family expressed in the developing nervous system in mice and *Drosophila*. *Mech. Dev.* **99**, 123-137.

Wang, W. and Lufkin, T. (2000). The murine *Otp* homeobox gene plays an essential role in the specification of neuronal cell lineages in the developing hypothalamus. *Dev. Biol.* **227**, 432-449.

Wang, W., VandeWater, T. and Lufkin, T. (1998). Inner ear and maternal reproductive defects in mice lacking the *Hmx3* homeobox gene. *Development* **125**, 621-634.

Wu, D. K., Nunes, F. D. and Choo, D. (1998). Axial specification for sensory organs versus non-sensory structures of the chicken inner ear. *Development* **125**, 11-20.

Yoshiura, K., Leysens, N. J., Reiter, R. S. and Murray, J. C. (1998). Cloning, characterization, and mapping of the mouse homeobox gene *Hmx1*. *Genomics* **50**, 61-68.